# A Variational Webster Solver For An Acoustic Graph Composed Of Interconnected Acoustic Ducts With Varying Cross-Section.

# Roland Van Praag 20 July 2022

#### Abstract

The sound field inside interconnected acoustic ducts with varying cross-section is modelled with a variational formulation of the Webster equation. The Sondhi model is used to take wall admitance and visto-thermal effects into account. The acoustic network of interconnected ducts is represented by a graph where each edge represents a duct described by a one-dimensional area function. We develop here numerical methods that allow us to solve the Webster equation in Laplace transform domain and to compute the transfer function between two given points of the acoustic graph. Resonances are obtained as eigenvalues of a matrix build with the area functions of the entire graph. Graph algorithms are used to identify subgraphs responsible for anti-resonances (zeros) of the transfer function. First, subgraphs that can be disconnected from any path joining input and output and that behave like Helmoltz resonators. Then we point out that subgraphs that contains cycles are also responsible for zeros in the transfer function. The first ones (disconnected) can, as the poles, be obtained by computing the eigenvalues of a matrix build with the area functions of the subgraph. The second ones (cycle) require more numerical analysis in order to be computed from the transfer function for being used in discrete time signal processing. Afterwards, we present experimental measurements that validate the results of our computations. We conclude by a discussion on the most appropriated numerical schemes for modelling acoustic properties of ducts that contains sharp constrictions. All numerical results presented here can be reproduced with Acwato software that can be downloaded here.

# Table of Contents

1	Aco 1.1 1.2 1.3	ustic model2One dimensional propagation in a lossless pipe2The Sondhi model2Boundary conditions3						
2	Variational formulation							
	2.1	Introduction						
	2.2	One single duct						
	2.3	Three ducts linked together						
3	Nur	nerical method						
	3.1	Introduction						
	3.2	The Rayleigh-Ritz method for a lossless single duct						
	3.3	Eigenmodes for a three ducts problem						
	3.4	Solutions for each value of the frequency						
	3.5	Acoustic graph						
	3.6	Verification of solutions						
	3.7	Eigenmodes for lossless tract						
	3.8	Solutions for a multi branch lossy tract						
4	The	transfer function 13						
	4.1	Solving the non homogeneous system						
	4.2	From poles and zeros of the lossless tract						
	4.3	Getting the zero frequencies						

	4.4	Numerical precision	14
	4.5	Generalization	15
	4.6	Pole-zero pair at origin	15
	4.7	Cycle zeros	17
	4.8	Wide band cycle zeros	18
5	Exp	perimental results	20
	5.1	Sharp constriction	20
	5.2	Resonator	22
	5.3	Cycle zeros	22
6	Nur	merical schemes	23
7	Con	aclusions	24
8	Ack	nowledgement	25

# 1 Acoustic model

# 1.1 One dimensional propagation in a lossless pipe

It can be shown that the wave equation in a long and narrow pipe becomes one-dimensional and takes the form of the following Webster equation

$$\frac{1}{A(x)}\frac{\partial}{\partial x}\left(A(x)\frac{\partial p(x,t)}{\partial x}\right) - \frac{1}{c^2}\frac{\partial^2 p(x,t)}{\partial t^2} = 0,\tag{1.1}$$

where A(x) and p(x,t) are the area cross section of the pipe and the pressure at a distance x from the pipe input and c is the speed of sound. By narrow, we mean that its diameter is smaller than its length. This result holds when A(x) varies little on distances in the same order of magnitude of the pipe width. The relationship between pressure and velocity  $\mathbf{v}$  is provided by the Euler equation [1, p 12]

$$\frac{\partial \mathbf{v}}{\partial t} + (\mathbf{v} \cdot \nabla) \mathbf{v} = -\frac{\nabla p}{\rho},\tag{1.2}$$

where  $\rho$  is the air density. Since we consider only small amplitude waves, the quadratic term in  $\mathbf{v}$  can been omitted. With the same one-dimensional approximation than for the Webster equation 1.1, Euler equation 1.2 becomes

$$\frac{\partial u(x,t)}{\partial t} + \frac{A(x)}{\rho} \frac{\partial p(x,t)}{\partial x} = 0, \tag{1.3}$$

with the volume velocity defined as u(x,t) = A(x)v(x,t).

If we work in the Laplace transform domain, the Webster equation 1.1 and the Euler equation 1.3 become

$$\frac{\partial}{\partial x} \left( A(x) \frac{\partial P(x,s)}{\partial x} \right) - \frac{s^2}{c^2} A(x) P(x,s), \tag{1.4}$$

$$\frac{\partial P(x,s)}{\partial x} + \frac{\rho s}{A(x)}U(x,s) = 0. \tag{1.5}$$

#### 1.2 The Sondhi model

The model used here for adding visco-thermal and wall effects to the Webster equation has been developed by Sondhi in order to decscribe the acoustic properties of the human vocal tract [2]. The simplest way to analyze the vocal tract acoustic properties is to assume that:

- (a) the wave motion in the vocal tract is planar and can be described by a one-dimensional equation,
- (b) the air viscosity and thermal conductivity are negligible,
- (c) the vocal tract walls are non-reacting (i.e: the walls are assumed to be rigid).

The Sondhi model allows us to relax assumptions (b) and (c) while keeping the formal problem very near to equation 1.4 that becomes

$$\frac{\partial}{\partial x} \left( A(x) \frac{\partial P(x,s)}{\partial x} \right) - \frac{\sigma^2(s)}{c^2} A(x) P(x,s) = 0, \tag{1.6}$$

where

$$\sigma^{2}(s) = s(s + \beta(s)), \quad \beta(s) = \frac{\omega_{0}^{2}}{(s+a)} + (c_{1}s)^{\frac{1}{2}}.$$
 (1.7)

where the parameters  $\omega_o$  and a take into account the wall reaction and  $c_1$  the visco-thermal losses. These parameters have been determined from experimental data for the human vocal tract:

$$\omega_0 = 406\pi \ rad/sec$$
,  $a = 130\pi \ rad/sec$  and  $c_1 = 4 \ rad/sec$ . (1.8)

Sondhi also shows (see section 4.2) that, if  $\hat{\omega}$  is a given resonance frequency of the lossless rigid-walled tract ( $\beta = 0$ ), the resonance frequency and bandwidth of the corresponding lossy reacting-walled are obtained by solving

$$\sigma^2 + \hat{\omega}^2 = s^2 + s\beta(s) + \hat{\omega}^2 = 0. \tag{1.9}$$

This last result is very important since, as will be seen later, poles and zeros of the lossless rigid-walled tract can be computed very efficiently and solving eq 1.9 provides us with the lossy reacting-walled ones that are required for designing discrete time signal processing filters that can be used for achieving real time articulatory speech synthesis. Moreover, since this result holds whatever the parameters  $\omega_o$ , a and  $c_1$  are, it also enables to model acoustic systems with different visco-thermal and wall effects.

## 1.3 Boundary conditions

We will here assume that the tract is terminated by a mass load at boundaries (x = 0 or x = L). The mass load condition is expressed as

$$\frac{P(x,s)}{U(x,s)} = \tau s,\tag{1.10}$$

where  $\tau$  is a constant which depends on the boundary opening. Here, we consider that the output radiation can be modeled by a vibrating piston set in a baffle. Keeping only the real term of lip impedance, we posit

$$\tau = \frac{\rho}{q\sqrt{A(x)}},\tag{1.11}$$

where  $q \sim 2.1$  for an infinite plan baffle [3]. Afterwards, q has been adjusted in order to better fit experimental data on human lips radiation and is obtained by the relation [4]

$$q = a\sqrt{A(x)} + b, (1.12)$$

where first estimations have lead to  $a = -3.5cm^{-1}$  and b = 35. Substituting 1.11 into 1.10 gives

$$U(x,s) = \frac{q\sqrt{A(x)}}{\rho s}P(x,s), \tag{1.13}$$

and therefore, if either a = b = 0 or A(x) = 0, we have

$$U(x,s) = 0, (1.14)$$

which corresponds to a closed end. Hence, the boundary condition 1.13 allows to implement both open and closed end boundary condition and to go from one to the other in a continuous way.

# 2 Variational formulation

#### 2.1 Introduction

Since the Webster Equation 1.6 with boundary conditions 1.13 or 1.14 has a Sturm-Liouville form, it can be deduced from a variational principle [5, p 119-120]. Simple junction conditions will allow us to connect several ducts together in order to compute the resonance frequencies and transfer functions for a vocal tract model in which nasal and sinus cavities may be taken into account [6].

# 2.2 One single duct

First of all, for convenience, we make the following variable change:

$$z = \frac{x}{L} \in [0, 1], \ f(x) \Longrightarrow \tilde{f}(z), \ \partial_x f(x) \Longrightarrow \frac{1}{L} \partial_z \tilde{f}(z).$$
 (2.1)

Henceforth, we will no longer overline the functions of z. Equations 1.5 and 1.6 become

$$\frac{1}{L}\frac{\partial P(z,s)}{\partial z} + \frac{\rho s}{A(z)}U(z,s) = 0, \qquad (2.2)$$

$$\frac{\partial}{\partial z}\left(A(z)\frac{\partial P(z,s)}{\partial z}\right) - \frac{\sigma^2L^2}{c^2}A(z)P(z,s) = 0. \tag{2.3} \label{eq:2.3}$$

Let us now consider the following functional:

$$S[z, P(z), \partial_z P(z)] = \int_{z_0}^{z_1} \mathcal{L}(z, P(z), \partial_z P(z)) dz + G_0(P(z_0)) + G_1(P(z_1)).$$
 (2.4)

From now, we will write S[P(z)] instead of  $S[z, P(z), \partial_z P(z)]$ . The functions P(z) which lead to extrema of this functional verify the following differential system [7, p 240-251]

$$\frac{\partial \mathcal{L}}{\partial P} - \frac{d}{dz} \frac{\partial \mathcal{L}}{\partial (\partial_z P)} = 0, \tag{2.5}$$

$$\frac{\partial \mathcal{L}}{\partial (\partial_z P)}|_{z_0} - \frac{\partial G_0}{\partial P(z_0)} = 0, \tag{2.6}$$

$$\frac{\partial \mathcal{L}}{\partial (\partial_z P)}|_{z_1} + \frac{\partial G_1}{\partial P(z_1)} = 0. \tag{2.7}$$

If we posit

$$\mathcal{L}(z, P, \partial_z P) = \frac{1}{L} A(z) \left[ (\partial_z P(z))^2 + \frac{L^2 \sigma^2}{c^2} P^2(z) \right], \tag{2.8}$$

S represents the action integral, and  $\mathcal{L}$  represents the Lagrangian of the pressure field inside the duct. Equation 2.5 with the Lagrangian 2.8 gives the wave equation 2.3. So, if  $G_0(P(z_0)) = G_1(P(z_1)) = 0$ , extremals of the action 2.4 with the lagrangian 2.8 are solutions of the wave equation 2.3 with implicit boundary conditions

$$[\partial_z P(z)]_{z=0} = [\partial_z P(z)]_{z=1} = 0,$$
 (2.9)

which gives the closed input condition 1.14, but not the open output condition 1.13. Indedd, substituting the closed input condition 1.14 into Euler equation 2.2 gives

$$[\partial_z P(z,s)]_{z=0} = 0 \,\forall s,\tag{2.10}$$

whereas substituting the output condition 1.13 yields

$$\frac{A(1)}{L} \left[ \frac{\partial P(z,s)}{\partial z} \right]_{z=1} + q\sqrt{A(1)}P(1,s) = 0.$$
 (2.11)

Conditions 2.10 and 2.11 are derived from equations 2.6 and 2.7 by positing

$$S = \int_0^1 \mathcal{L}(z, P, \partial_z P) dz + q \sqrt{A(1)} P^2(1).$$
 (2.12)

The variational formulation presented here for a duct open at the output end (oral vowels), remains available for a duct closed at both ends (voiced labial occlusive) without having to redefine the functional. Indeed, if A(1) = 0 (duct closed at lips), the functional S (eq 2.12) automatically takes the required form for a duct closed at both ends.

## 2.3 Three ducts linked together

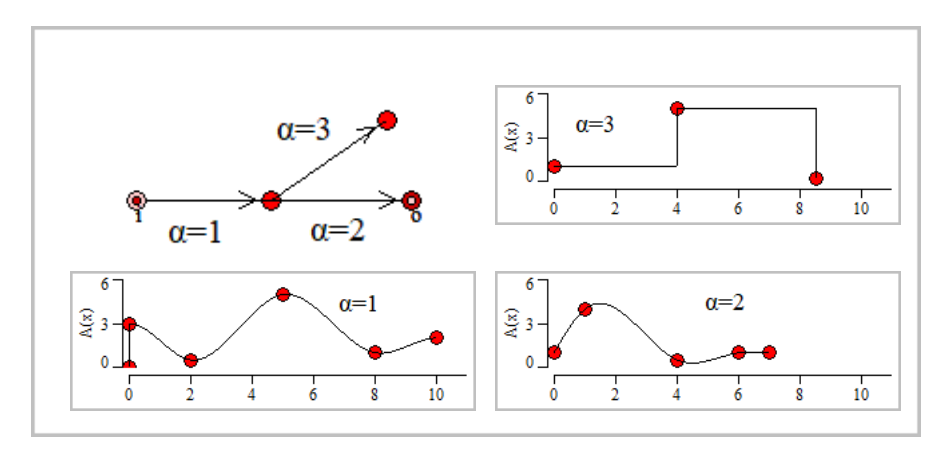


FIGURE 2.1 – Three ducts connected represented by their area functions

Now, we are going to formulate the problem when three ducts are connected [8]. First of all, we will associate an area function to each duct and name it  $A_{\alpha}(z)$ ,  $\alpha = 1, 2, 3$ . (see fig 2.1).

Then we build the following action integral associated to each of the three area functions denoted by  $\alpha$ 

$$I_{\alpha} = \int_{0}^{1} \frac{1}{L_{\alpha}} A_{\alpha}(z) \left[ \left( \partial_{z} P_{\alpha}(z) \right)^{2} + \frac{L_{\alpha}^{2} \sigma^{2}}{c^{2}} P_{\alpha}^{2}(z) \right] dz, \tag{2.13}$$

where  $L_{\alpha}$  is the length of the duct  $\alpha$ .

We now introduce simple physical junction conditions which are pressure continuity and flow conservation expressed respectively as

$$P_1(1) = P_2(0) = P_3(0),$$
 (2.14)

$$\frac{A_1(1)}{L_1}\partial_z P_1(1) = \frac{A_2(0)}{L_2}\partial_z P_2(0) + \frac{A_3(0)}{L_3}\partial_z P_3(0). \tag{2.15}$$

Now, aiming to get a variational formulation of the wave equation 2.3, inside any duct, we built one functional  $S_{\alpha}$  for each of the three tracts. Let

$$S_1[P_1; P_2, P_3] = I_1 - 2P_1(1) \left[ \frac{A_2(0)}{L_1} \partial_z P_2(0) + \frac{A_3(0)}{L_3} \partial_z P_3(0) \right],$$
 (2.16)

$$S_{2}[P_{2}; P_{1}, P_{3}] = I_{2} + 2P_{2}(0) \left[ \frac{A_{1}(1)}{L_{1}} \partial_{z} P_{1}(1) - \frac{A_{3}(0)}{L_{3}} \partial_{z} P_{3}(0) \right] + \xi P_{2}(0) \left[ 2P_{1}(1) - P_{2}(0) \right] + q \sqrt{A_{2}(1)} P_{2}^{2}(1),$$
(2.17)

$$S_{3}[P_{3}; P_{1}, P_{2}] = I_{3} + 2P_{3}(0) \left[ \frac{A_{1}(1)}{L_{1}} \partial_{z} P_{1}(1) - \frac{A_{2}(0)}{L_{2}} \partial_{z} P_{2}(0) \right]$$

$$+ \xi P_{3}(0) \left[ 2P_{1}(1) - P_{3}(0) \right] + q \sqrt{A_{3}(1)} P_{3}^{2}(1),$$

$$(2.18)$$

where  $\xi$  is an arbitrary constant  $(\neq 0)$  and  $S_1[P_1; P_2, P_3]$  means that only the function  $P_1$  may vary inside the functional  $S_1$ . The two other functions  $P_2$  and  $P_3$  are considered as fixed for this functional. Considering the variational problem

$$\frac{\delta S_1}{\delta P_1} = 0, \quad \frac{\delta S_2}{\delta P_2} = 0, \quad \frac{\delta S_3}{\delta P_3} = 0, \tag{2.19}$$

and applying the differential system (equations 2.5, 2.6 and 2.7) to each of the functional  $S_1$ ,  $S_2$  and  $S_3$ , we obtain the required wave equation 2.3 for each duct, the junction conditions 2.14 and 2.15, the radiation conditions (lips and nostrils) for the duct  $\alpha = 2$  and  $\alpha = 3$  and the glottis condition for the duct  $\alpha = 1$ . We notice here that, for a given i, a term containing  $\partial_z P_i$  cannot occur outside the integral of the corresponding action  $S_i$ . We see for example that the boundary term of action  $S_1$  contains only terms in  $\partial_z P_2$  and  $\partial_z P_3$  and, from the variational point of view, those derivatives are constant for the action  $S_1$ . We also notice that the flow conservation is imposed on  $S_1$  an so, considering that this conservation is also obtained on  $S_2$  and  $S_3$ , the pressure continuity is imposed on those last two actions for each non-null value taken by  $\xi$ .

# 3 Numerical method

### 3.1 Introduction

In this section, we will only consider lossless and rigid walled ducts because, in the framework of the Sondhi model, loss and wall effects can be treated afterwards. Indeed, resonance frequencies and bandwidths of a lossy, reacting walled duct can be deduced from resonance frequencies of the lossless, rigid walled corresponding duct by solving equation 1.9. For a lossless rigid walled tract, we have  $\omega_0 = a = c_1 = 0$  and thus  $\beta = 0$  (see equations 1.7). Since  $s = i\omega$ , we have  $\sigma^2 = -\omega^2$  and the wave equation 2.3 becomes

$$\partial_z \left( A_\alpha(z) \partial_z P_\alpha(z) \right) + \frac{\omega^2 L_\alpha^2}{c^2} A_\alpha(z) P_\alpha(z) = 0, \tag{3.1}$$

for each duct  $\alpha$  included in the problem. The complex equation ( $\sigma^2$  instead of  $-\omega^2$ ) will be treated in section 3.8. We will see that the variational formulation allows us to compute the resonance frequencies first for one single duct and then for a multi duct system. After that we will check if the numerical approximations of solutions verify the wave equation with required boundary conditions.

# 3.2 The Rayleigh-Ritz method for a lossless single duct

We assume here that the solution may be approximated by the development

$$P(z) = \sum_{i=1}^{n} C_i \eta_i(z),$$
 (3.2)

where  $\eta_i(z)$  i=1,...,n are n functions chosen in a convenient complete set of linearly independent functions. Here, we have chosen the n firsts Tchebychev polynomials. Substituting Lagrangian 2.8 into action 2.12 and replacing P by its development 3.2 gives

$$S = \int_{0}^{1} \frac{1}{L} A(z) \left\{ \left( \sum_{i=1}^{n} C_{i} \eta_{i}'(z) \right) \left( \sum_{j=1}^{n} C_{j} \eta_{j}'(z) \right) - \frac{L^{2} \omega^{2}}{c^{2}} \left( \sum_{i=1}^{n} C_{i} \eta_{i}(z) \right) \left( \sum_{j=1}^{n} C_{j} \eta_{j}(z) \right) \right\} dz$$

$$+ q \sqrt{A(1)} \left( \sum_{i=1}^{n} C_{i} \eta_{i}(z) \right) \left( \sum_{j=1}^{n} C_{j} \eta_{j}(z) \right),$$
(3.3)

where  $\eta'(z)$  denotes  $\partial_z \eta(z)$ . Then, the functional S becomes an ordinary quadratic function with respect to the coefficients  $C_i$ . Because we are looking for the extremals of this action, we ask

$$\frac{\partial S}{\partial C_i} = 0 \quad \forall i \in [1, \ n]. \tag{3.4}$$

Since,

$$\frac{\partial}{\partial C_i} \sum_{j=1}^n C_j \eta_j(z) = \sum_{j=1}^n \delta_{ij} \eta_j = \eta_i \text{ and } \frac{\partial}{\partial C_i} \sum_{j=1}^n C_j \eta_j'(z) = \sum_{j=1}^n \delta_{ij} \eta_j' = \eta_i', \tag{3.5}$$

where

$$\delta_{ij} = \begin{cases} 1 & \text{if } i = j, \\ 0 & \text{otherwise,} \end{cases}$$
 (3.6)

for each i = 1, ..., n, we obtain

$$\frac{1}{L} \sum_{j=1}^{n} C_{j} \int_{0}^{1} A(z) \left\{ \eta_{i}'(z) \eta_{j}'(z) - \lambda \frac{L^{2}}{c^{2}} \eta_{i}(z) \eta_{j}(z) \right\} + q \sqrt{A(1)} \sum_{j=1}^{n} C_{j} \eta_{i}(1) \eta_{j}(1) = 0.$$
 (3.7)

where  $\lambda = \omega^2$ . The resulting system is now written

$$\sum_{j=1}^{n} (V_{ij} - \lambda W_{ij}) C_j = 0, \tag{3.8}$$

where  $V_{ij}$  and  $W_{ij}$  are given by

$$V_{ij} = \frac{1}{L} \int_0^1 A(z) \eta_i'(z) \eta_j'(z) dz + q \sqrt{A(1)} \eta_i(1) \eta_j(1) , \qquad (3.9)$$

$$W_{ij} = \frac{L}{c^2} \int_0^1 A(z) \eta_i(z) \eta_j(z) dz.$$
 (3.10)

The system 3.8 may be written on the following matrix form

$$(W^{-1}V - \lambda \mathbb{1})\overline{C} = \overline{0}, \tag{3.11}$$

1 denoting the identity matrix and  $\overline{C}$  is the vector whose components are the  $C_i$ . Such homogeneous system has non-trivial solutions if and only if  $\lambda$  is eigenvalue of the matrix  $W^{-1}V$ . The corresponding eigenvector  $\overline{C}$  provides the resonance mode by substituting its components into equation 3.2.

# 3.3 Eigenmodes for a three ducts problem

We will now consider the three functionals  $S_1$ ,  $S_2$  and  $S_3$  given by equations 2.16, 2.17 and 2.18 and pose, for each value of  $\alpha \in \{1, 2, 3\}$ 

$$P_{\alpha}(z) = \sum_{i=N_{+}+1}^{N_{\alpha}+n_{\alpha}} C_{i} \eta_{i_{\alpha}}(z) , \quad N_{\alpha} = \sum_{i=1}^{\alpha-1} n_{i} , \quad (N_{1}=0), \quad i_{\alpha} = i - N_{\alpha}$$
 (3.12)

Now, we ask

$$\frac{\partial S_{\alpha}}{\partial C_{i}} = 0, \quad \forall i \in [N_{\alpha} + 1, N_{\alpha} + n_{\alpha}]$$
(3.13)

 $n_{\alpha}$  being the number of coordinate functions chosen for the duct  $\alpha$  and  $N = \sum_{\alpha} n_{\alpha}$ , the number of coefficients  $C_i$ .

For each value of  $\alpha$ , eq 3.13 represents  $n_{\alpha}$  equations with N unknowns. For  $\alpha=1$ , the last equation respects the fact that  $P_2$  and  $P_3$  are considered as fixed for the action  $S_1$ . For  $\alpha=2$ ,  $P_1$  and  $P_3$  fixed for  $S_2$  and so on. Equation 3.13 eventually becomes one system of N equations and N unknowns

$$\sum_{i=1}^{N} (V_{ij} - \lambda W_{ij}) C_j = 0, \tag{3.14}$$

which may be written under the form

$$(W^{-1}V - \lambda \mathbb{1})\overline{C} = 0. \tag{3.15}$$

As example, here we compute the coupling terms with duct  $\alpha = 2$  in action  $S_1$ :

$$-2P_{1}(1)\frac{A_{2}(0)}{L_{2}}\partial_{z}P_{2}(0) = -2\frac{A_{2}(0)}{L_{2}}\left(\sum_{k=1}^{n_{1}}C_{k}\eta_{k_{1}}(1)\right)\left(\sum_{j=n_{1}+1}^{n_{1}+n_{2}}C_{j}\eta_{j_{2}}^{'}(0)\right)$$

$$\xrightarrow{(\frac{\partial}{\partial C_{i}}\ \forall\ i=1,\dots,n_{1})}$$

$$-2\frac{A_{2}(0)}{L_{2}}\eta_{i_{1}}(1)\sum_{j=n_{1}+1}^{n_{1}+n_{2}}C_{j}\eta_{j_{2}}^{'}(0) = \sum_{j=n_{1}+1}^{n_{1}+n_{2}}C_{j}\left(-2\frac{A_{2}(0)}{L_{2}}\eta_{i_{1}}(1)\eta_{j_{2}}^{'}(0)\right)$$

$$\Rightarrow V_{ij} = -2\frac{A_{2}(0)}{L_{2}}\eta_{i_{1}}(1)\eta_{j_{2}}^{'}(0) \quad \forall\ i \in [1,n_{1}], \quad j \in [n_{1}+1,n_{1}+n_{2}].$$

$$(3.16)$$

The resulting matrices V and W are detailed in fig 3.1.

The resonance frequencies are given by the eigenvalues of the matrix  $W^{-1}V$ . The solutions  $P_1, P_2$  and  $P_3$  are finally obtained by substituting the corresponding eigenvector coefficients into 3.12.

## 3.4 Solutions for each value of the frequency

As will be shown in section 4.1, the tansfer function is given by the volume velocity at the output  $U_2(1,s)$  while having imposed unit volume velocity at the input  $U_0(0,s) = 1$ . With this input condition, we can compute the transfer function by computing the pressure field and the volume velocity at the output for each value of the frequency.

The Euler equation 2.2 with  $U_0(0,s) = 1$  gives

$$\frac{A_1(0)}{L_1}\partial_z P_1(0,s) = -\rho s U_1(0,s) = -\rho s. \tag{3.17}$$

$$\mathbf{V} = \begin{bmatrix} 1, & \dots & & & & \\ \frac{2}{L_1} \int_0^1 A_1(z) [\eta_{i_1}'(z) \eta_{j_1}'(z)] dz & -\frac{2A_2(0)}{L_2} \eta_{i_1}(1) \eta_{j_2}'(0) & -\frac{2A_3(0)}{L_3} \eta_{i_1}(1) \eta_{j_3}'(0) \\ \\ \frac{2A_1(1)}{L_1} \eta_{i_2}(0) \eta_{j_1}'(1) & \frac{2}{L_2} \int_0^1 A_2(z) [\eta_{i_2}'(z) \eta_{j_2}'(z)] dz & -\frac{2A_3(0)}{L_3} \eta_{i_2}(0) \eta_{j_3}'(0) \\ \\ +2\xi \eta_{i_2}(0) \eta_{j_1}(1) & -2\xi \eta_{i_2}(0) \eta_{j_2}(0) & \\ +2q \sqrt{A_2(1)} \eta_{i_2}(1) \eta_{j_2}(1) & \\ \\ \frac{2A_1(1)}{L_1} \eta_{i_3}(0) \eta_{j_1}'(1) & -\frac{2A_2(0)}{L_2} \eta_{i_3}(0) \eta_{j_2}'(0) & \frac{2}{L_3} \int_0^1 A_3(z) [\eta_{i_3}'(z) \eta_{j_3}'(z)] dz \\ \\ +2\xi \eta_{i_3}(0) \eta_{j_1}(1) & -2\xi \eta_{i_3}(0) \eta_{j_2}'(0) & \frac{2}{L_3} \int_0^1 A_3(z) [\eta_{i_3}'(z) \eta_{j_3}'(z)] dz \\ \\ -2\xi \eta_{i_3}(0) \eta_{j_3}(0) & -2\xi \eta_{i_3}(0) \eta_{j_3}(1) & \\ \end{bmatrix}$$

	$\frac{2L_1}{c^2} \int_0^1 A_1(z) \eta_{i_1}(z) \eta_{j_1}(z) dz$	0	0
$\mathbf{W} =$	0	$\frac{2L_2}{c^2} \int_0^1 A_2(z) \eta_{i_2}(z) \eta_{j_2}(z) dz$	0
	0	0	$\frac{2L_3}{c^2} \int_0^1 A_3(z) \eta_{i_3}(z) \eta_{j_3}(z) dz$

Figure 3.1 – Detail of matrices V and W

This condition is obtained using eq 2.7 by adding the term  $-2\rho s P_1(0,s)$  to the functional  $S_1$  (eq 2.16). In this case, the calculation in section 3.3 gives instead of system 3.14

$$\sum_{j=1}^{N} (V_{ij} - \lambda W_{ij}) C_j = G_i, \tag{3.18}$$

where  $\lambda = -\sigma^2$ ,  $\sigma$  is given by eq 1.7. and

$$G_i = \begin{cases} 2\rho s \ \eta_i(0) & \forall i = 1, \dots, n_1 \\ 0 & \text{otherwise.} \end{cases}$$
 (3.19)

This system is no longer homogeneous and has a solution for each value of  $\lambda$  except for the eigen values of  $W^{-1}V$ , for which the matrix  $V - \lambda W$  is no more invertible.

## 3.5 Acoustic graph

This method can now be extended to an arbitrary number of ducts interconnected by imposing pressure continuity and flow conservation at each junction [9]. From now, we will used terms from graph theory glossary such as *edge*, *vertex*, *graph*, *subgraph*, *path* whose definitions can be found in graph theory book such as [10].

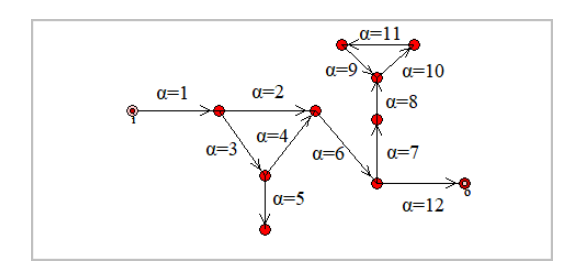


FIGURE 3.2 – Acoustic graph representation : each edge represents a duct whose geometry is described by an area function. The arrows show the x direction of the area function.

#### 3.6 Verification of solutions

Now, we would like to check if the approximated solutions obtained by this method for a lossless rigid-walled acoustic graph ( $\lambda = \omega^2$ ) verify both the wave equation and its boundary conditions. The lossy reacting-walled case will be discussed in section 3.8.

This will be done with two types of area functions as illustrated by fig 2.1:

- Cubic splines for continuous area functions.
- Step functions more appropriated for disontinued area functions.

Let a single duct be described by its area function A(z). We want here to check if the function P(z) obtained by this method verifies equation 3.1. In order to do this we define the error on the solution  $E_w(s)$  by

$$E_w(s) = \sqrt{\frac{\int_0^1 \left[ A(z)P(z) + \frac{c^2}{\lambda L^2} \partial_z \left( A(z) \partial_z P(z) \right) \right]^2 dz}{\int_0^1 (A(z)P(z))^2 dz}} , \tag{3.20}$$

where the term inside the integral on numerator is expected to be 0 if the Webster equation is verified, whereas the denominator normalizes the error  $E_w$  to a relative value. For each duct extremity, we have to check if the boundary conditions we imposed match the numerical solution we have obtained. In the case of the solution of the non homogeneous system 3.18 for a given value of the frequency, the volume velocity at the input should be  $U_i(z_i, s) = 1$ ,  $z_i$  beeing the z coordinate at input (0 or 1). We therefore define the input error

$$E_i(s) = U(z_i, s) - 1. (3.21)$$

If the **vertex** of the acoustic graph corresponding to the duct extremity is an opened end, we have to check the impedance at the duct end. We define boundary error for open boundaries at the point  $z_o(0 \text{ or } 1)$  as the difference between the obtained impedence an the target impendance defined by equation 1.10

$$E_o(s) = \frac{\frac{P(z_o, s)}{U(z_o, s)} - Z_{target}}{|Z_{target}|} = \frac{\frac{P(z_o, s)}{U(z_o, s)} - \tau s}{|\tau s|}.$$
(3.22)

If the considered boundary is closed at the point  $z_c$  ( $A(z_c) = 0$  in eq 1.13), the target impedance is  $\infty$ , we will use the inverse of impedance as error since in that case, it should be 0.

$$E_c(s) = \frac{U(z_c, s)}{P(z_c, s)} \tag{3.23}$$

When a duct extremity has more than one duct connected, it is a junction  $vertex \ \mathbf{p_j}$  at  $z_j$ , we must check errors on pressure continuity and flow conservation. We define the error on pressure continuity as

$$E_p(s) = \frac{\max(P_{\alpha}(z_j)) - \min(P_{\alpha}(z_j))}{\max(P_{\alpha}(z_j))},$$
(3.24)

where  $max(P_{\alpha}(z_j))$  is the maximum of pressure computed at each duct extremity connected to the considered **vertex** and  $min(P_{\alpha}(z_j))$  is the minimum of pressure at the same **vertex**.

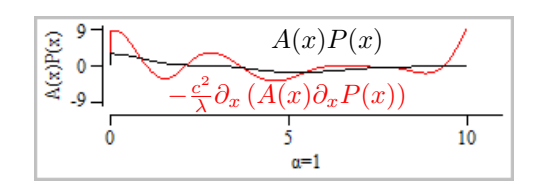
We define the error on flow conservation as

$$E_f(s) = \frac{\sum_{\alpha \in \mathbf{p_j}} sgn(\alpha) \frac{A_{\alpha}(z_{\alpha})}{L_{\alpha}} \partial_z P_{\alpha}(z_{\alpha})}{\sum_{\alpha \in \mathbf{p_j}} \left| \frac{A_{\alpha}(z_{\alpha})}{L_{\alpha}} \partial_z P_{\alpha}(z_{\alpha}) \right|}, \tag{3.25}$$

where  $sgn(\alpha) = 1$  if the duct is connected to the **vertex** from its start  $(z_{\alpha} = 0)$  and  $sgn(\alpha) = -1$  if it is connected from its end  $(z_{\alpha} = 1)$ .

## 3.7 Eigenmodes for lossless tract

Here, we will check that the eigenmodes obtained by solving eq 3.14 verify both the lossless Webster equation 3.1 and boundary conditions. If we consider that the approximation obtained by the variational method is corrupted only by small but fast oscillations around the exact solution, its derivative will be stained by significant errors. So,  $E_w(s)$  being obtained by using second derivative is considerable as can be seen in fig 3.3 that shows the forth resonance mode in the duct  $\alpha = 1$  of the acoustic graph described in fig 2.1.



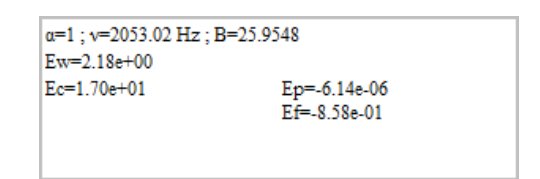


FIGURE 3.3 – Comparison of the two terms of the Webster equation for an eigenmode at 2053.02Hz and corresponding errors.

Consequently, we will avoid derivating the obtained approximation by integrating the wave equation. Indeed, integration of equation 3.1 between 0 and  $z \in [0, 1]$  gives

$$A(z)\partial_z P(z) + F(z) + C_1 = 0,$$
 (3.26)

where  $C_1$  is an integration constant and F(z) is defined as

$$F(z) = \frac{\lambda L^2}{c^2} \int_0^z A(\xi) P(\xi) d\xi. \tag{3.27}$$

Now, we compute the integration constant  $C_1$  in order to minimize the left term of equation 3.26 at least mean square all along the duct length and so, we minimize the quantity

$$E_{tot}(P) = \int_0^1 (A(z)\partial_z P(z) + F(z) + C_1)^2 dz,$$
 (3.28)

by asking

$$\frac{\partial E_{tot}(P)}{\partial C_1} = 0, (3.29)$$

which yields

$$C_1 = -\int_0^1 (A(z)\partial_z P(z) + F(z)) dz.$$
 (3.30)

And we can now compute the mass flow using integration less sensitive to small oscillations using

$$A(z)\partial_z P(z) = -F(z) - C_1, \tag{3.31}$$

and therefore, using the Euler equation 2.2

$$U(z,s) = \frac{-F(z) - C_1}{\rho s L}. (3.32)$$

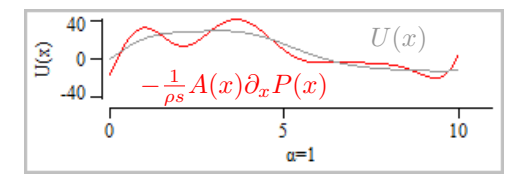


Figure 3.4 – Comparison between volume velocities using derivative and using U(x) from eq. 3.32.

Now, we would like to check if the derivative computed by integration (eq 3.31) represents a good approximation of the exact wave function derivative. To do this, we integrate the wave equation a second time. Integrating equation 3.26 between 0 and  $z \in [0, 1]$  leads to

$$\int_0^z A(\xi)\partial_\xi P(\xi)d\xi + \int_0^z F(\xi)d\xi + C_1 z + C_2 = 0,$$
(3.33)

where  $C_2$  is a second integration constant. Integrating the first term of eq 3.33 by parts gives

$$A(z)P(z) - \int_0^z (\partial_{\xi} A(\xi)) P(\xi) d\xi + \int_0^z F(\xi) d\xi + C_1 z + C_2 = 0, \tag{3.34}$$

which, for z = 0 gives

$$C_2 = -A(0)P(0). (3.35)$$

So we can check the accuracy of our solutions by comparing A(z)P(z) with

$$\widetilde{AP}(z) = \int_0^z (\partial_{\xi} A(\xi)) P(\xi) d\xi - \int_0^z F(\xi) d\xi - C_1 z - C_2.$$
 (3.36)

If stepwise area functions are used to describe the acoustic graph geometry:

$$A(z) = A_i \quad \forall \ z_i < z < z_{i+1} : i = 0, ..., n,$$
 (3.37)

and if we want to apply the previous method to such functions, we have to use the delta Dirac distribution in order to compute the second term in equation 3.34. So

$$\partial_z A(z) = \begin{cases} (A_i - A_{i-1})\delta(z - z_i) & \text{if } z = z_i, \\ 0 & \text{otherwise,} \end{cases}$$
 (3.38)

where the Dirac delta function  $\delta(z)$  is defined by

$$\delta(z) = \begin{cases} \infty & \text{if } z = 0, \\ 0 & \text{otherwise,} \end{cases}$$
 (3.39)

$$\int_{-\epsilon}^{+\epsilon} \delta(z)dz = 1 \text{ and } \int_{a-\epsilon}^{a+\epsilon} \delta(z-a)\Psi(z)dz = \Psi(a) \quad \forall \ \epsilon > 0.$$
 (3.40)

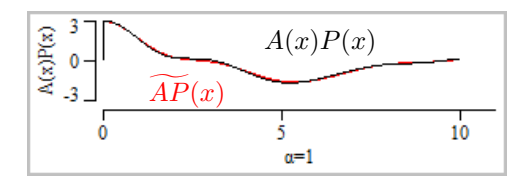
That gives

$$\int_0^z (\partial_{\xi} A(\xi)) P(\xi) d\xi = \sum_{i \mid z_i < z} (A_i - A_{i-1}) P(z_i).$$
 (3.41)

Therefore, we can now check the wave equation without using approximation derivatives, except to obtain the first integration constant (see eq 3.30). We define  $\widetilde{E}_w(s)$  the same way as  $E_w(s)$  by

$$\widetilde{E}_{w}(s) = \sqrt{\frac{\int_{0}^{1} (A(z)P(z) - \widetilde{AP}(z))^{2} dz}{\int_{0}^{1} (A(z)P(z))^{2} dz}}.$$
(3.42)

The error definitions 3.22 and 3.23, remain unchanged but U(x,s) is computed using 3.32 instead of 2.2. The error on pressure continuity is unchanged and error on flow conservation is computed by substituting eq 3.31 in 3.25.



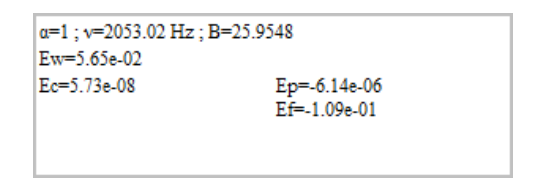


FIGURE 3.5 – Comparison between A(x)P(x) and  $\widetilde{AP}(x)$ 

Comparing figure 3.3 and 3.5, we see that the two curves much better match and  $E_w$  is highly reduced. Here, we have used  $n_1 = n_2 = n_3 = 8$  and, if we either increase the number of base functions or check a lower frequency mode, the two curves matching is even better. Errors on boundary conditions ( $E_c$ ,  $E_p$  and  $E_f$ ) also show a great improvements. Moreover, the output error ( $E_o$ ) for the duct  $\alpha = 2$  decreases from  $-3.26 \ 10^{-1}$  to  $-9.23 \ 10^{-9}$ .

Nevertheless, the error on flow conservation remains significant. This occurs once one of the ducts connected to the junction exhibits strong area function variations. We will see in section 6 that this problem can be solved by modifying our numerical scheme.

#### 3.8 Solutions for a multi branch lossy tract

If we want to compute the transfer function for each value of the frequency, we have to solve eq 3.18 where  $\lambda$  and the  $C_j$  coefficients are complex numbers. The technique used in section 3.7 is here developed in the complex case. When losses have to be taken into account, equation 3.1 must be replaced by equation 2.3. Now, because  $\sigma^2$  is a complex number, equation 2.3 has to be solved in the complex domain with

$$\lambda = -\sigma^2 = \lambda_r + i\lambda_i \quad \text{and} \quad P(z) = P_r(z) + iP_i(z). \tag{3.43}$$

Consequently, equation 2.3 is split into real and imaginary parts given by

$$\partial_z \left( A(z) \partial_z P_r(z) \right) + A(z) \frac{L^2}{c^2} \left( \lambda_r P_r(z) - \lambda_i P_i(z) \right) = 0, \tag{3.44}$$

$$\partial_z \left( A(z) \partial_z P_i(z) \right) + A(z) \frac{L^2}{c^2} \left( \lambda_r P_i(z) + \lambda_i P_r(z) \right) = 0. \tag{3.45}$$

That gives A(z)P(z) as functions of its derivatives

$$A(z)P_r(z) = \frac{-c^2}{L^2(\lambda_r^2 + \lambda_i^2)} \left\{ \lambda_r \partial_z (A(z)\partial_z P_r(z)) + \lambda_i \partial_z (A(z)\partial_z P_i(z)) \right\}$$
(3.46)

$$A(z)P_i(z) = \frac{-c^2}{L^2(\lambda_r^2 + \lambda_i^2)} \left\{ \lambda_r \partial_z (A(z)\partial_z P_i(z)) - \lambda_i \partial_z (A(z)\partial_z P_r(z)) \right\}$$
(3.47)

The coefficients of the Chebyshev series expansion  $P(z) = \sum_j C_j \eta_j(z)$  are now complex :  $C_j = C_j^r + i C_j^i$ . Real and imaginary parts of solutions are given by

$$P_r(z) = \sum_{j} C_j^r \eta_j(z) \; ; \; P_i(z) = \sum_{j} C_j^i \eta_j(z).$$
 (3.48)

Integrating equations 3.44 and 3.45 gives us

$$A(z)\partial_z P_{(r,i)}(z) + F_{(r,i)}(z) + C_{1(r,i)} = 0, (3.49)$$

where the subscript (r, i) means that the equation actually represents two equations : one with the subscript r and and other with the subscript i with

$$F_r(z) = \frac{L^2}{c^2} \int_0^z A(\xi) \left\{ \lambda_r P_r(\xi) - \lambda_i P_i(\xi) \right\} d\xi, \tag{3.50}$$

$$F_i(z) = \frac{L^2}{c^2} \int_0^z A(\xi) \left\{ \lambda_r P_i(\xi) + \lambda_i P_r(\xi) \right\} d\xi, \tag{3.51}$$

 $C_{1r}$  and  $C_{1i}$  being two integration constants.

Minimizing discrepancies to equations 3.49 at least mean square gives

$$C_{1(r,i)} = -\int_0^1 \left[ A(z)\partial_z P_{(r,i)}(z) + F_{(r,i)}(z) \right] dz. \tag{3.52}$$

Substituting equation 3.49 into Euler equation 2.2 gives

$$U(z,s) = -\frac{(F_r(z) + C_{1r}) + i(F_i(z) + C_{1i})}{\rho s L}.$$
(3.53)

Integrating equations 3.49 gives

$$A(z)P_{(r,i)}(z) - \int_0^z \partial_{\xi}(A(\xi))P_{(r,i)}(\xi)d\xi + \int_0^z F_{(r,i)}(\xi)d\xi + C_{1(r,i)}z + C_{2(r,i)} = 0,$$
 (3.54)

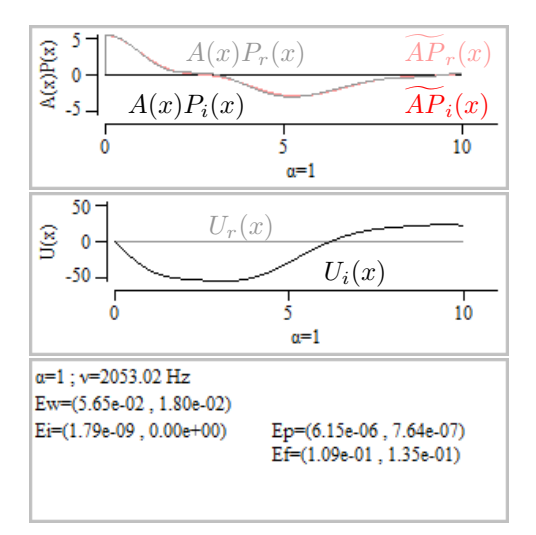
which, for z = 0 gives

$$A(0)P_{(r,i)}(0) = -C_{2(r,i)}, (3.55)$$

and equation 3.36 becomes

$$\widetilde{AP}_{(r,i)}(z) = \int_0^z \partial_{\xi}(A(\xi)) P_{(r,i)}(\xi) d\xi - \int_0^z F_{(r,i)}(\xi) d\xi - C_{1(r,i)} z - C_{2(r,i)}. \tag{3.56}$$

All errors defined in section 3.6  $(E_w, E_i, E_o, E2_c, E1_g, E2_g, E_p \text{ and } E_f)$  become complex numbers.



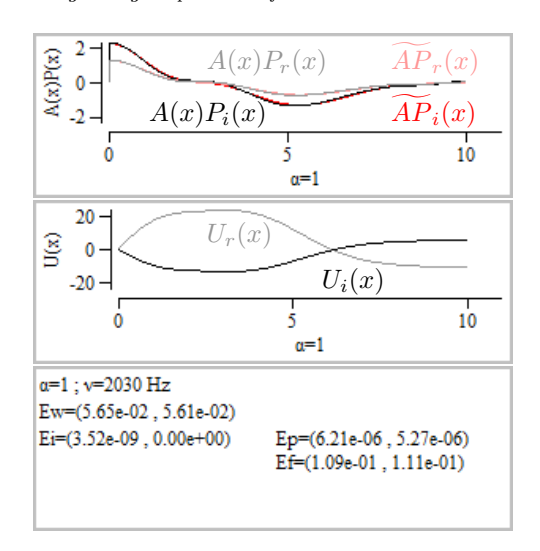


Figure 3.6 – Solution in the duct  $\alpha = 1$  of the lossy acoustic graph in fig 2.1 at resonance frequency 2053.02Hz (left) and away from it at 2030Hz (right).

The left side of figure 3.6 shows the solution for a lossy tract computed with the default Sondhi parameteres obtained by solving equation 3.18 in the complex domain at resonance frequency 2053.02Hz. The real part of each function is plotted in light colour. In that case, we see that P(x,s) is nearly real wheras U(x,s) is nearly imaginary. As can be seen on the right side of fig 3.6, if we move away from the resonance, both real and imaginary parts of P(x,s) and U(x,s) become significant.

# 4 The transfer function

# 4.1 Solving the non homogeneous system

The transfer function can be defined as the ratio, in the Laplace transform domain, of the volume velocity at the output  $U_o(s) = U(1, s)$  to the volume velocity at the input  $U_i(s) = U(0, s)$ 

$$H(s) = \frac{U_o(s)}{U_i(s)},\tag{4.1}$$

which is equivalent to the Laplace transform of the response at the output to a volume velocity impulsion at the input at time t = 0. Indeed, if

$$u(0,t) = \delta(t), \tag{4.2}$$

then, from de Diract  $\delta$  definition (3.39)

$$U_i(s) = U(0, s) = \int_0^\infty \delta(t)e^{-st}dt = e^0 = 1,$$
(4.3)

and so, in this case the transfer function is given by  $U_o(s)$ . Substituting the impulse response condition 4.3 into Euler equation 2.2 yields to the boundary condition

$$\left[\frac{A(z)}{L}\partial_z P(z)\right]_{z=0} = -\rho s U(0,s) = -\rho s, \tag{4.4}$$

that requires solving the non homogeneous system 3.18. For each value of  $\lambda$  (so for each  $s = i\omega$ ), we can compute the solutions of complex Webster equation 2.3 by computing the solutions of the system 3.18 and substitute them into eq 3.48. Equations 4.1, 4.3, 2.2 and 3.53 give

$$H(s) = U_o(1,s) = -\frac{A_l(1)}{\rho s L_o} \partial_z P_o(1,s)$$

$$= \frac{1}{\rho L_o s} \left[ (F_r(1,s) + C_{1r}) + i(F_i(1,s) + C_{1i}) \right]. \tag{4.5}$$

## 4.2 From poles and zeros of the lossless tract

The transfer function can also be expressed in terms of its poles and zeros :

$$\widetilde{H}(s) = H_0 \prod_{k=1}^{n_p} \frac{p_k p_k^*}{(s - p_k)(s - p_k^*)} \prod_{l=1}^{n_z} \frac{(s - z_l)(s - z_l^*)}{z_l z_l^*} , \qquad (4.6)$$

where the  $p_k$  are the  $n_p$  first poles and  $z_l$  the  $n_z$  first zeros of the acoustic system. Zeros occur when subsidiary tracts are connected to the main tract by imposing pressure continuity and flow conservation at tract connections (see section 3.3).

Thanks to the Sondhi model, once we have computed the poles and zeros of the lossless rigid-walled acoustic system, we can compute the corresponding poles and zeros of the lossy reacting-walled one by solving equation 1.9

$$s^2 + s\beta(s) + \hat{\omega}^2 = 0.$$

Using the newton method for finding the zeros of a non linear function and taking  $s=i\hat{\omega}$  as starting point for the Newton algorithm provides solutions in few iterations. Moreover, since our main goal is to achieve real time articulatory speech synthesis, poles and zeros are all what is required to implement discrete time signal processing filters as described in [11, p. 296].

Hence, we first compute the poles and zeros of the lossless acoustic  $\operatorname{graph}(\hat{\omega})$ . Then we solve equation 1.9 to obtain the corresponding lossy ones and substitute the resulting  $p_k$  and  $z_k$  into eq 4.6. The constant  $H_0 = H(0)$  needed to compute the transfer function this way is obtained by the previous method but this time, we have only to solve the system 3.18 once instead of solving it for each frequency value. After that, computation of H(s) is much more faster using equation 4.6. As seen in section 3.3, the resonance frequencies of the lossless acoustic graph are given by the eigenvalues of the matrix  $W^{-1}V$ .

# 4.3 Getting the zero frequencies

As can be seen on the orange curve in fig 4.1 obtained with the acoustic graph from figure 2.1, once a tract ( $\alpha=3$ ) is connected to the Input/Output  $\operatorname{path}$  ( $\alpha=1,\ \alpha=2$ ), the lossless transfer function  $\widehat{H}(s)$ , computed with eq 4.5 but with  $\omega_0=a=c_1=0$ , has not only poles but also zeros. In such a case, the non homogeneous solutions (section 3.8 with  $\lambda_i=0$ ) at the frequencies corresponding to the zeros, have  $P_2(z,s)=U_2(z,s)=0$   $\forall z$  in the output duct ( $\alpha=2$ ). Therefore, the pressure continuity at junction requires  $P_1(1,s)=P_3(0,s)=P_2(0,s)=0$ . We therefore identify the zero of the transfer function to the poles of the duct  $\alpha=3$  where a null pressure is imposed at the input. The output boundary condition 2.11 does not allows to impose P=0 but we can impose a disconnection impedance  $Z_d$  as small as we want but not zero by adding the term  $\zeta P_3^2(0,s)$ ,  $\zeta$  beeing a large number, to the functional  $S_3$  in equation 2.18 where connection terms have been removed. This yields by eq 2.6 to the boundary condition

$$\frac{A_3(0)}{L_3}\partial_z P_3(0,s) + \zeta P_3(0,s) = -\rho s U_3(0,s) + \zeta P_3(0,s) = 0, \tag{4.7}$$

and hence the disconnection impedance is given by,

$$Z_d = \frac{P_3(0,s)}{U_3(0,s)} = \frac{\rho s}{\zeta}.$$
(4.8)

We also define the error on disconnection impendance the same way we defined the error on output impedance in eq 3.22 with

$$E_d(s) = \frac{\frac{P_3(0,s)}{U_3(0,s)} - Z_d}{|Z_d|} = \zeta \frac{\frac{P_3(0,s)}{U_3(0,s)} - \frac{\rho s}{\zeta}}{|\rho s|}.$$
 (4.9)

In the example used here, we have set  $\zeta = 10^6$ . The algorithm used to compute the fast transfer

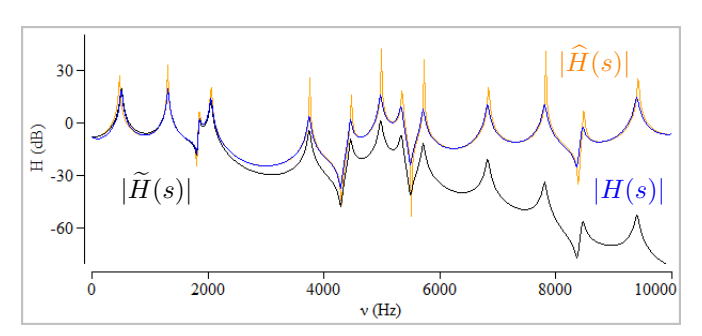


Figure 4.1 – modules of  $\widehat{H}(s)$ , H(s) and  $\widetilde{H}(s)$  computed for the acoustic **graph** in fig 2.1 with the number of bases functions  $n_1 = n_2 = n_3 = 8$ 

function H(s) using 4.6 is eventually:

- Compute the poles of the lossless tract by calculating the eigenvalues of the matrix  $W^{-1}V$ .
- Build the  $V_3$  and  $W_3$  matrices for the subtract  $\alpha = 3$  with boundary condition 4.7 and compute the eigen values of the matrix  $W_3^{-1}V_3$  that are identified to the lossless zeros.
- Compute the lossy poles and zeros by solving eq 1.9 for each pole and zero found previously.
- Substitute the resulting  $p_k$ 's and  $z_l$ 's into equation 4.6

Comparing the resulting transfer functions  $\widetilde{H}(s)$  and H(s) in figure 4.1, we see that both poles, zeros and bandwith are correct but  $\widetilde{H}(s)$  shows a strong damping at high frequencies.

# 4.4 Numerical precision

We can see in fig 4.2, where the number of bases functions has been increased to 10 that the damping is reduced, high frequecies poles and zero are moved and new ones occur. This is normal since, for a high frequency solution, the highest degree base function must have at least as much oscillation that the sound field for that frequency. Moreover, the size of the matrices, and therefore the maximum number of eigen values, must be at least the number of poles or zeros in the frequency range we are interested in.

If  $n_i$  exceeds 10, products of Chebyshev polynomials that are used for building the matrices V and W in fig 3.1 become high degree polinomials with large coefficients that can lead to floating point overflow.

The method used here for connecting three ducts together can also be used for connecting two. Therefore, when a duct is too long for modelling high frequency sound field with n base functions, it is

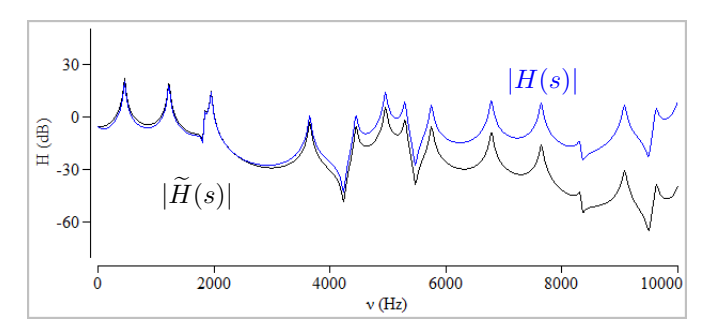


FIGURE 4.2 – modules of H(s) and  $\widetilde{H}(s)$  computed for the acoustic **graph** in fig 2.1 with the number of bases functions  $n_1 = n_2 = n_3 = 10$ 

split into several parts that are linked together by imposing pressure continuity and flow conservation at the junctions. The result obtained by splitting each duct into three parts is shown in fig 4.3. The acoustic graph eventually contains 9 ducts and the V and W matrix size is 9 x 8 = 72.

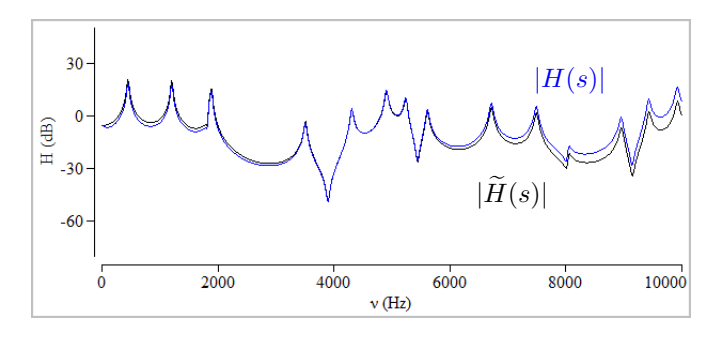


FIGURE 4.3 – modules of H(s) and  $\widetilde{H}(s)$  computed for the acoustic **graph** in fig 2.1 with the number of bases functions  $n_i = 8 \,\forall i$  but each duct is split into 3 pieces.

## 4.5 Generalization

Zeros as decribed in sec 4.3 are generated by any *induced connected subgraph* of the acoustic *graph* representation having the following properties:

- The *subgraph* does not contains any *edge* that is included in any IO *path*. An IO *path* is a *path* that connects the input to the output.
- ullet The subgraph contains one and only one disconnecting  $vertex\ \mathbf{v_d}$  that belongs to at least one IO path
- If we remove all edges of the subgraph that include the disconnecting  $vertex \ \mathbf{v_d}$ , the acoustic graph is split into two components.

We call such **subgraph** a disconnected **subgraph** whose examples are illustrated in fig 4.4. The area functions corresponding the the **graph edges** used here are simple pipes with constant area cross section.

The good matching between H(s) and  $\tilde{H}(s)$  illustrated by figure 4.4 shows that the zeros have correctly been identified since there is no assumption on there origin in the computation of H(s).

#### 4.6 Pole-zero pair at origin

When losses are are considered, and mainly when the first resonance frequency is low, if we look closely at the frequencies just above zero, we observe a sharp but shallow damping on the transfer function H that is not modelled by its pole-zero approximation  $\widetilde{H}$ . An example is shown in fig 4.5. Since it does not occur on lossless cases, lossy poles and zeros that would model this behaviour cannot be deduced from the lossless case.

Since  $H(\nu)$  has a pole like shape areound the frequency origin, we want to add a pole with ferquency  $\nu=0$  and a bandwidth  $B_p$  to the transfer function approximation  $\widetilde{H}(\nu)$ . If we only add a second order pole to the transfer function it will show a strong damping at high frequencies. The range of the damping due to the pole can be limitted by adding a zero at frequency  $\nu=0$  and a bandwith  $B_z>B_p$ . We therefore consider the new approximation

$$H(s) \simeq \frac{(s - z_o)(s - z_o^*)}{z_o z_o^*} \frac{p_o p_o^*}{(s - p_o)(s - p_o^*)} \widetilde{H}(s),$$
 (4.10)

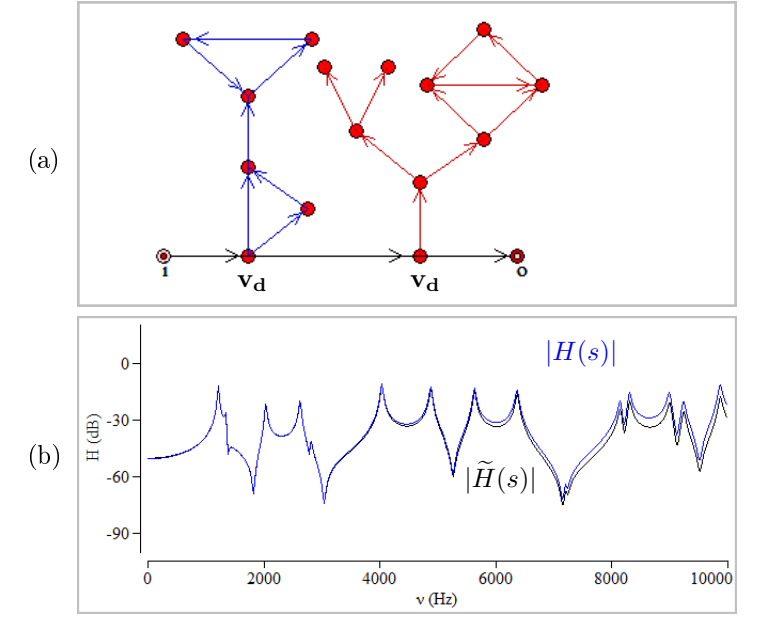


FIGURE 4.4 – (a) Acoustic **graph** with two disconnected **subgraphs** (one in red, the other in blue) responsible for zeros in the transfer function from input (i) to output (o). (b) module of corresponding H(s) and  $\widetilde{H}(s)$ 

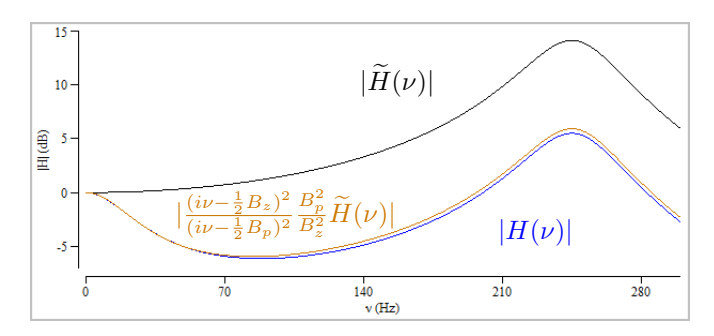


FIGURE 4.5 – modules of  $H(\nu) = H(s = 2i\pi\nu)$ ,  $\widetilde{H}(\nu)$  and its multiplication by an appropriated pole-zero pair at  $\nu = 0$ .

with  $s = i\omega = 2i\pi\nu$ ,  $p_o = \pi B_p$  and  $z_o = \pi B_z$ , it becomes

$$H(s = i\omega = 2i\pi\nu) \simeq \frac{(i\nu - \frac{1}{2}B_z)^2}{(i\nu - \frac{1}{2}B_p)^2} \frac{B_p^2}{B_z^2} \widetilde{H}(2i\pi\nu)$$
 (4.11)

If we take the norm of both side of the equation, we get

$$\frac{\sqrt{\frac{1}{16}B_z^4 + \nu^4 + \frac{1}{2}B_z^2\nu^2}}{\sqrt{\frac{1}{16}B_p^4 + \nu^4 + \frac{1}{2}B_p^2\nu^2}} \frac{B_p^2}{B_z^2} - H_s(\nu) = 0, \ H_s(\nu) = \frac{|H(2i\pi\nu)|}{|\widetilde{H}(2i\pi\nu)|}$$
(4.12)

Hence, if we compute  $|H(\nu)|$  and  $|\widetilde{H}(\nu)|$  for 2 values of the frequency  $\nu$ , equation 4.12 gives a system of 2 equations with 2 unknowns:  $B_p$  and  $B_z$ . This can be solved numerically using a 2D Newton's method. The 2D Newton search requires correct initial values of  $B_p$  and  $B_z$ . The first estimation of  $B_p$  is obtained using a  $2^{nd}$  degree polynomial approximation around a pole at frequency  $\nu_p$ 

$$\begin{split} H_{s}(\nu) & \simeq p(\nu) = a\nu^{2} + b\nu + c. \\ a & = \frac{1}{2}\partial_{\nu}^{2}H_{s}(\nu_{p}), \\ b & = \partial_{\nu}H_{s}(\nu_{p}) - 2a\nu_{p} = -2a\nu_{p} \ (\nu_{p} \text{ is extremum}), \\ c & = H_{s}(\nu_{p}) - a\nu_{p}^{2} - b\nu_{p}. \end{split} \tag{4.13}$$

By definition of the bandwidth around  $\nu_p = 0$ , we have

$$H_s(\nu_p \pm \frac{1}{2}B_p) = \frac{1}{\sqrt{2}} H_s(\nu_p) \xrightarrow{\nu_p=0} H_s(\frac{1}{2}B_p) = \frac{1}{\sqrt{2}} H_s(0).$$
 (4.14)

If  $\nu_b$  is the lowest root of the  $2^n d$  degree polynomial

$$\sqrt{2p(\nu)} - H_s(0) = 0, \tag{4.15}$$

the first estimation of  $B_p$ , and  $B_z$  for the 2D Newton search obtained from eq 4.12 are estimated empirically from  $\nu_b$  and the first resonance frequency.

We therefore need 5 computations of H using eq 4.5:

- 3 for getting  $H(\nu = 0)$  and its two first derivatives that give  $H_0$  in eq 4.6 and the first estinamtion of  $B_p$ .
- 2 for building the system from eq 4.12 whose solution are the bandwidths of  $p_o$  and  $z_o$  in eq 4.10.

From now,  $\widetilde{H}$  designs the transfer function approximation that includes such pole-zero pair when they are found.

## 4.7 Cycle zeros

Occurence of *cycles* int the *graph* can also lead to zeros in the transfer function. The acoustic *graphs* used to highlight this behavior are illustrated by fig 4.6 representing 4 acoustic *graphs* with the same *edges* and *vertices*. The 3 firsts only differ by the length of the pipe  $\alpha = 2$ . The  $4^{th}$  one differs from the  $3^{rd}$  one by the input  $(\alpha = 1)$  and output  $(\alpha = 5)$  pipe lengths. The *edges* of the *graph* represent uniform pipes defined by their cross section  $A_{\alpha}$  and their length  $L_{\alpha}$ . Note that the area cross section of the pipes included in the cycle  $(\alpha = 2, 3 \text{ or } 4)$  is half of the pipes that include input  $(\alpha = 1)$  and output  $(\alpha = 5)$  so that  $A_1(L_1) = A_2(0) + A_3(0) = A_2(L_2) + A_4(L_4) = A_5(0)$ .

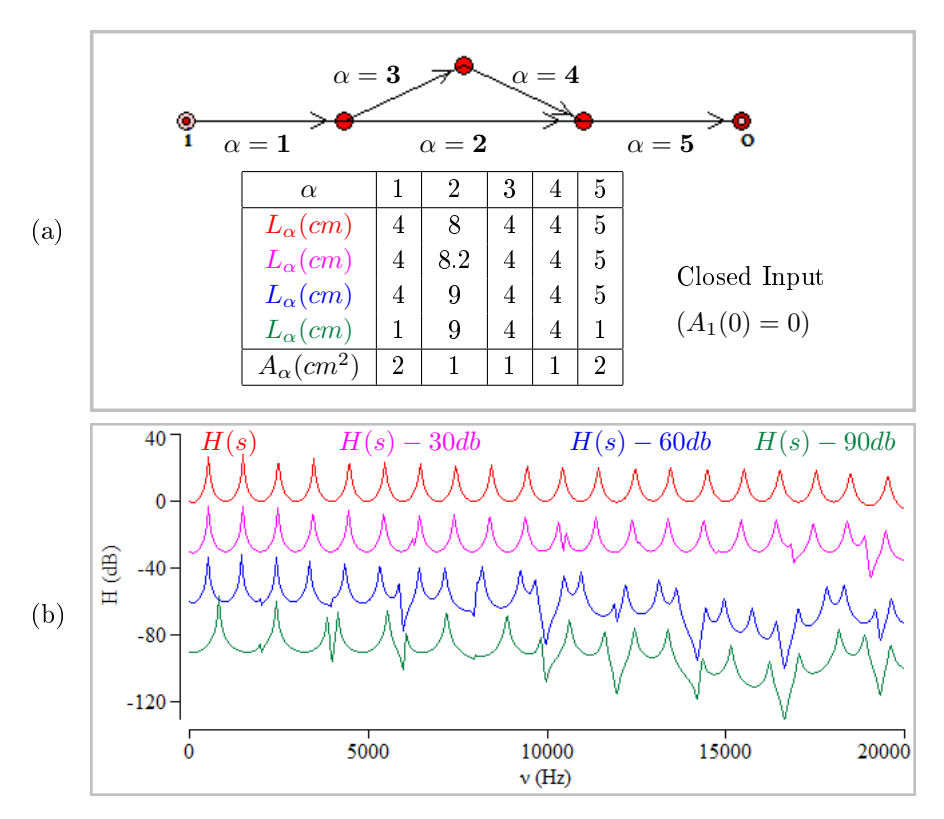


FIGURE 4.6 – (a) Acoustic *graph* with one *cycle* responsible for zeros in the transfer function from input (i) to output (o). (b) corresponding H(s) and  $\widetilde{H}(s)$  for the 4 configurations in the table in fig (a).

We can see in fig 4.6 that when  $L_2 = L_3 + L_4 = 8$ , the corresponding transfer function H(s) is the same that for a uniform pipe with closed input and of length 17 cm with an area cross section of 2  $cm^2$  where poles are around 500, 1500, 2500.... Once  $L_2$  differs a little from  $L_3 + L_4$  pole-zero pairs occur in the transfer function as can be seen on H(s) corresponding to  $L_2 = 8.2$ . If the length difference increases as on the curve H(s) corresponding to  $L_2 = 9$ , poles and zeros from a pair move away from each other and new pole-zero pairs occur. For the last curve H(s) for which we have shortened the pipes connected to the input and output, we see that the poles have changed from H(s) but not the zero. The zeros depend only on the area functions corresponding to the edges include in the eggele.

We have analyzed the solutions as described in section 3.8 for a lossless tract at zero frequencies detected graphically. In such cases, we observed that the impedance at the end of the pipe  $\alpha=1$  is allso independent of the input pipe length but vary in a non-linear and non-mononic way with regard to the frequency and we were unable to find a boundary condition such as eq 4.7 in order to identify the zero values as eigenvalues of a linear system.

We therefore implemented a numerical search for finding such zeros. First of all, in order to reduce computation time, we build a new acoustic graph that includes all the  $cycle\ edges$  and vertices. Then we add a small pipe at both input and output of the cycle. We can see in fig 4.7 (a) that the module of the corresponding transfer function  $\hat{H}(s)$  shape is not appropriated for a Newton search. Since we can compute the poles of the transfer function with the eigenvalue method, we can cancel these poles by multiplying the transfer function by a function that has zeros for each of them and we define

$$\hat{\bar{H}}_p(s) = \hat{\bar{H}}(s) \prod_{k=1}^{n_p} \frac{(s - \hat{\bar{p}}_k)(s - \hat{\bar{p}}_k^*)}{\hat{\bar{p}}_k \hat{\bar{p}}_k^*}, \tag{4.16}$$

where  $\hat{H}(s)$  is the transfer function of the lossless graph containing only the cycle and two small pipes added at its input and output and the  $\hat{p}_k$ 's are the poles of this acoustic graph. We can see in fig 4.7 (a) that the module of  $\hat{H}_p(s)$  has now only zeros and has phase shifts only at the zero frequencies. We extracted the zero by implementing a dichotomic search on phase shifts of  $\hat{H}_p(s)$ . Computation of all zeros in fig 4.7 with a precision of  $10^{-3}$  Hz required 272 computation of  $\hat{H}(s)$  using eq 4.5.

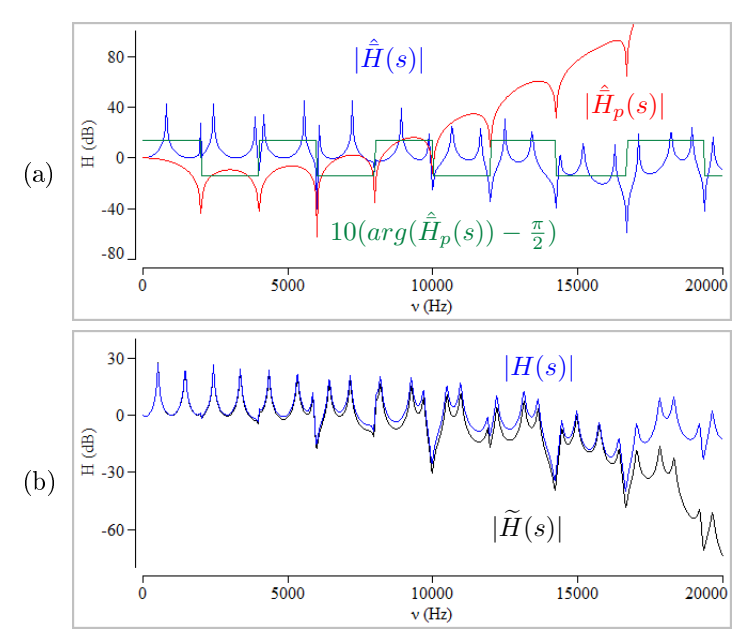


FIGURE 4.7 – (a) Illustration of the computation of the zeros from the  $3^{rd}$  acoustic graph in fig 4.6 were only the cycle has been kept and small pipes have been added at input and output sides. (b) Resulting transfer functions for the entire  $3^{rd}$  graph.

The result obtained by computing the poles of the entire graph, and taking losses into account by solving eq 1.9 for both the poles and the zeros obtained by the phase shift search is shown in fig 4.7 (b) where a good matching between the pole and zero bandwidths is again observed.

## 4.8 Wide band cycle zeros

Now, we connect a pipe opened at both ends with a length of 8.5 cm and a constant area cross section of  $2 cm^2$  at the intersection of the pipes  $\alpha=3$  and  $\alpha=4$  of the last acoustic graph ( $L_2=9$ ) represented in fig 4.6 (a). If we apply the method used to obtain the fig 4.7 (b), the resulting transfer function  $\widetilde{H}_{wb}(s)$  in fig 4.8 (a) exhibits wide band poles the are not present in H(s). As we cancelled the poles in eq 4.16, we now cancel the null bandwidth zeros by defining

$$\hat{\bar{H}}_{zp}(s) = \hat{\bar{H}}_p(s) \prod_{l=1}^{n_z} \frac{\hat{\bar{z}}_l \hat{z}_l^*}{(s - \hat{\bar{z}}_l)(s - \hat{\bar{z}}_l^*)} , \qquad (4.17)$$

where the  $\hat{z}_l$  are the zeros obtained by the phase shift search method.

The residual function  $\hat{H}_{zp}(s)$  contains only the wide band zeros whose frequencies can easily be extracted by a Newton search on its derivative. The starting values for the search are extracted from the transfer function value set stored while computing the phase shift search. Computation of the zeros by phase shift search of  $\tilde{H}_{wb}(s)$  in fig 4.8 (a) required 327 computation of H(s) and computation of the 4 wide band zeros required only 29 more computations.

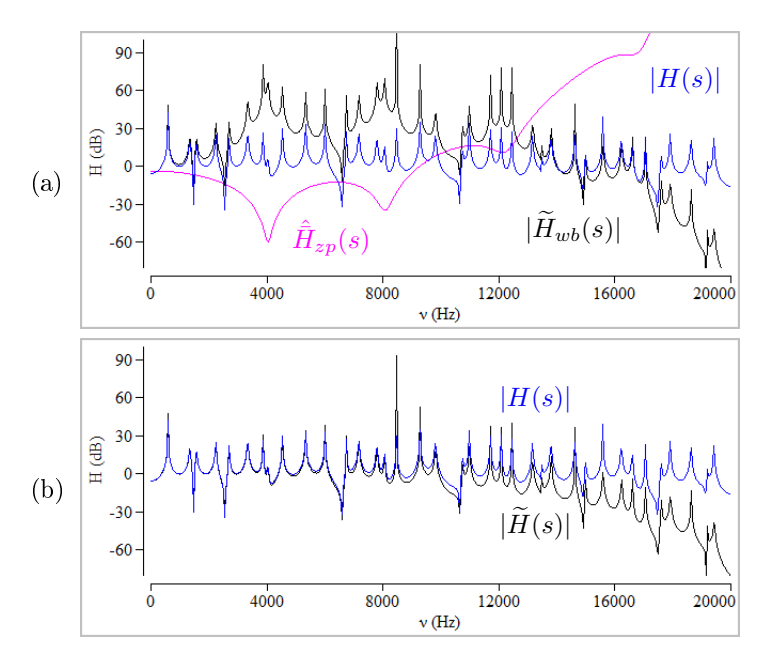


FIGURE 4.8 – (a) Illustration of the computation of the wide band zeros from the acoustic *graph* in fig 4.6 with and added pipe at the intersection of pipes  $\alpha = 3$  and  $\alpha = 4$ . (b) Resulting transfer functions.

Since the Newton search on the derivative of  $\hat{H}_{zp}(s)$  also requires computation of its second derivative, we evaluate the bandwith by approximating the transfer function around a given wide band zero at frequency  $\nu_z$  with a  $2^{nd}$  order polynomyal

$$|\hat{H}_{zp}(\nu)| = |\hat{H}_{zp}(s = i2\pi\nu)| \simeq p(\nu) = a\nu^{2} + b\nu + c$$

$$a = \frac{1}{2} \left. \partial_{\nu}^{2} |\hat{H}_{zp}(\nu)| \right|_{\nu = \nu_{z}},$$

$$b = \left. \partial_{\nu} |\hat{H}_{zp}(\nu)| \right|_{\nu = \nu_{z}} - 2a\nu_{z} = -2a\nu_{z},$$

$$c = |\hat{H}_{zp}(\nu_{z})| - a\nu_{z}^{2} - b\nu_{z},$$

$$(4.18)$$

We must also note that the imaginary part of the residual function  $\tilde{H}_{zp}(s)$  is always 0. If we add one  $2^{nd}$  order wide band zero to the transfer function  $\tilde{H}_{wb}(s)$ , it will exhibit a phase transition arround the zero frequency that does not match the observed constant phase behavior. Instead, we can add two second order zeros, the second one having a negative real part. i.e:

$$\frac{(i\omega - (\sigma_z + i\omega_z))(i\omega - (\sigma_z - i\omega_z))(i\omega - (-\sigma_z + i\omega_z))(i\omega - (-\sigma_z - i\omega_z))}{(\sigma_z + i\omega_z)(\sigma_z - i\omega_z)(-\sigma_z + i\omega_z)(-\sigma_z - i\omega_z)}$$

$$= \frac{((\omega - \omega_z)^2 + \sigma_z^2)((\omega + \omega_z)^2 + \sigma_z^2)}{(\omega_z^2 + \sigma_z^2)^2}, \tag{4.19}$$

that is a real function and therefore matches our requirement.

Since the bandwith  $B_z$  of a single  $2^{nd}$  order zero at frequency  $\nu_z$  is defined by  $|\hat{\bar{H}}_{zp}(\nu_z \pm \frac{1}{2}B_z)| = \sqrt{2} |\hat{\bar{H}}_{zp}(\nu_z)|$ , when two such zeros are located at the same frequency, we must have  $|\hat{\bar{H}}_{zp}(\nu_z \pm \frac{1}{2}B_z)| = 2 |\hat{\bar{H}}_{zp}(\nu_z)|$ . We therefore search for the values of  $\tilde{\nu}_z$  such as  $p(\tilde{\nu}_z) = 2 |\hat{\bar{H}}_{zp}(\nu_z)|$  which is equivalent to searching the two roots of the  $2^{nd}$  degree equation

$$p(\nu) - 2|\hat{\bar{H}}_{zp}(\nu_z)| = 0,$$
 (4.20)

which is straightforward and the banwidth approximation is finally given by

$$B_z = 2(\nu_z - \tilde{\nu}_z) , \ \sigma_{zl} = \pi B_z .$$
 (4.21)

where  $\tilde{\nu}_z$  is the lowest of the two roots of eq 4.20. Adding two wide band zeros for each of such zero found to  $\widetilde{H}_{wb}(s)$  finally gives a good matching as can be seen in fig 4.8 (b).

We must here point out that when applying to a lossy acoustic  $\operatorname{graph}_{\lambda}$  equation 1.9 must not be used to transform the last wide band zeros. They must be inserted in  $\widetilde{H}(s)$  as it is in order to have the good matching with H(s). This remark also holds when poles of the lossless tract have a bandwidth. This occurs if the real matrix  $W^{-1}V$  has complex conjugate pairs of eigenvalues.

We can finally generalize our method: any *induced connected subgraph* of the acoustic *graph* found by the following method are casusing zeros as described in this section.

- Find all cycles in the *graph*.
- Gather cycles that have at least one *edge* in common.
- ullet Keep resulting subgraphs that have at least one edge on an IO path
- Identify any *vertex*  $\mathbf{v_{dc}}$  that belong to only one such a *subgraph* and is connected to at least one *edge*  $\mathbf{e_{dc}}$  that does not belong neither to any IO *path* nor to any cycle.
- Find all vertices that can be joined by a path that starts with  $\{\mathbf{v_{dc}}, \mathbf{e_{dc}}\}$  and adjoin all edges and vertices contained in such path to the subgraph containing  $\mathbf{v_{dc}}$ .

An example with a *graph* containing two such *subgraphs* and resulting the transfer functions H(s) and  $\widetilde{H}(s)$  are shown in fig 4.9

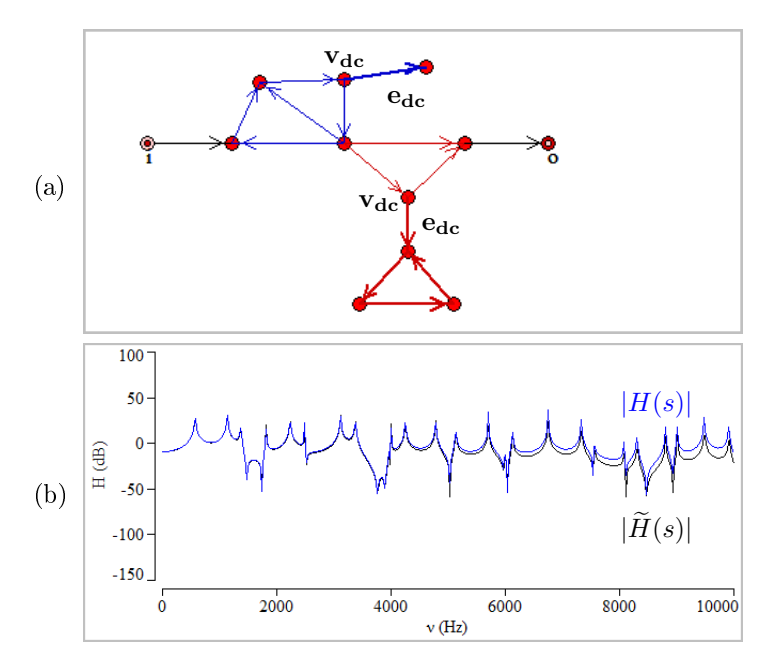


FIGURE 4.9 – (a) Acoustic *graph* with two *cycle subgraphs* (one in red, the other in blue) responsible for zeros in the transfer function from input (i) to output (o). (b) module of corresponding H(s) and  $\widetilde{H}(s)$ 

# 5 Experimental results

We have seen in sections 3.8 and 3.7 that we can compute the solutions of the Webster equation and its eigenmodes for an assembly of interconnected acoustic ducts with variable area cross section.

In section 5.1, we will show that our method can be used for modelling sharp constriction though the Webster equation is not appropriated when the area function strongly varies on short distance.

In section 5.2 we will see that the acoustic properties of a resonator connected to a uniform pipe is properly modelled by connecting three ducts using the variational formulation as developed in section 3.3

In section 5.3 we will show that the zeros resulting from cycles in the acoustic graph as predicted in section 4.7 are confirmed by experimental results.

In order to measure the transfer function for the three cases discussed here, we closed the input of the devices with a thin plastic film stretched as a drum's hide on which we tapped with a finger as impulse source. A microphone is placed near the output in order to record the impulse response.

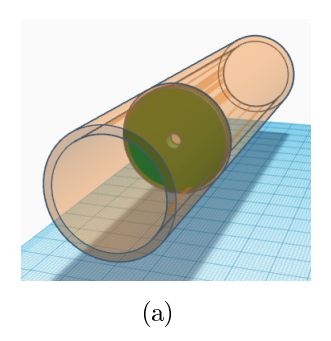
## 5.1 Sharp constriction

We have seen in section 1.1 that the Webster equation 1.1 holds if the pipe diameter is smaller compared to its length and the area function A(x) varies little on distances in the same order of

magnitude of the pipe width.

Yet, we want compute the resonances and anti-resonances of acoustic systems for which that constraint does not hold like the one described by its area function in fig 5.1 (b). The area cross section of the constriction is  $\simeq 0.2\,cm^2$  compared to the  $\simeq 7\,cm^2$  for the rest of the pipe. Its width is  $4\,mm$ 

Experimental device for testing cycle zeros can be build with simple PVC plumbing materials as will be seen in section 5.3. We did not find such materials for building devices including sharp constrictions. Hence, in this section and the following one, they were built using a 3D printer. The Tinkercad design of the device and the corresponding area function are shown in fig 5.1 (a).



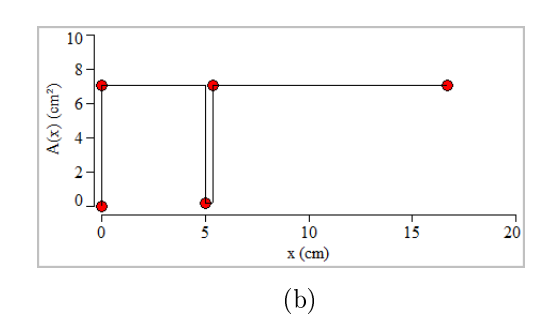


FIGURE 5.1 - (a) Design of the device used to measure the transfer function of a duct with a sharp constriction. (b) The corresponding area function

Since the output is not a plane baffle and the plastic used in the 3D printer has not the same wall properties as a vocal tract. We first adjust the output (section 1.3) and wall (section 1.2) parameters by measuring the resonances of a simple pipe made with the same diameter and material. The output radiation parameters have been set to a = -2.5; b = 12 and the Sondhi parameters to  $\omega_0 = 200 \, rad/s$ ;  $a = 400 \, rad/s$ ;  $c_1 = 50 \, rad/s$ .

If we compute the resonances corresponding to the area function in fig 5.1 using the method described in section 3.2, we get nearly the same values as the ones obtained for a uniform tube. This does not match the transfer function of such a duct (see grey curve on fig 5.2).

Since the method used in section 3.3 for connecting three ducts can also be used for connecting two, we can also represent the area function in fig 5.1 (a) as 3 uniform pipes connected together by imposing flow conservation and pressure continuity at boundaries. This leads to the black curve in fig 5.2 that get closer to the measured spectrum though the two first resonances are still too high.

The Webster and Sondhi equations are obtained by integrating the pressure and velocity fields across the area cross section of the duct. Since the velocity is actually 0 at wall boundaries, we introduced a radius correction parameter that reduces the area cross section. If the area cross section is A(x), we compute the transfer function  $\widetilde{H}'(s)$  with the reduced area function A'(s) defined as:

$$\widetilde{H}'(s) = \widetilde{H}(s)|_{A(x) \to A'(x)} \text{ with } A'(x) = \pi \left(\sqrt{\frac{A(x)}{\pi}} - \delta r\right)^2$$
(5.1)

This finally leads to the orange curve in fig 5.2 with  $\delta r = 0.07 \, cm$ .

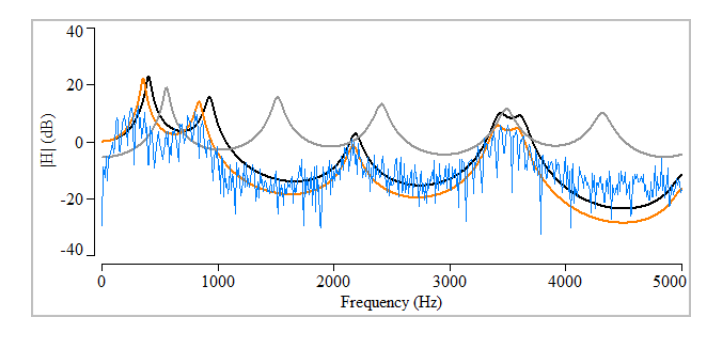


FIGURE 5.2 – Spectrum measured at the output of the device represented in fig 5.1 (a) (blue). Module of the transfer function corresponding to the area function plotted in fig 5.1 (b) (grey). Module of the transfer function computed by splitting the same area function into three uniform pipes connected by imposing the pressure continuity and flow conservation at boundaries (black). Module of the transfer function computed for the three pipes with the modified area function  $\widetilde{H}'(s)$  with  $\delta r = 0.07\,cm$  (orange)

#### 5.2 Resonator

In this section, we will check that the method developed in section 3.3 properly describes the acoustic of a pipe to which a resonator is connected. The experimental device is shown in fig 5.3 (a). Since the material is the same than in section 5.1, we used the same Sondhi parameters:  $\omega_0 = 200 \, rad/s$ ;  $a = 400 \, rad/s$ ;  $c_1 = 50 \, rad/s$ . The output parameters have be adapted to a pipe with smaller area cross section to a = -2; b = 7.5.

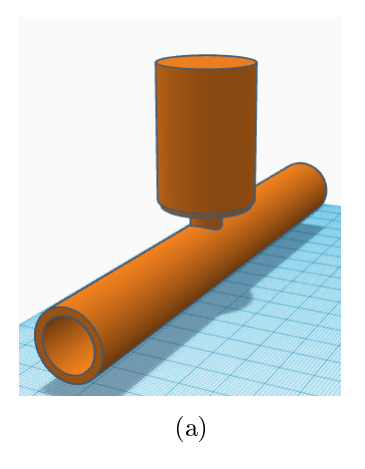
The result is shown in fig 5.4 where the Fourier transform of the signal output is plotted in blue. The grey curve is obtained by using the area function defined in equation 5.2, the black curve is obtained by splitting  $A_3(x)$  into two pipes connected as in section 5.1 and the orange curve is obtained by reducing the area function using equation 5.1

$$A_{1}(x) = \begin{cases} 0 & \text{if } x = 0\\ 2.01 & \text{if } 0 < x \le 8.5 \end{cases}$$

$$A_{2}(x) = 2.01 & \text{if } 0 \le x \le 7.5$$

$$A_{3}(x) = \begin{cases} 0.2 & \text{if } 0 \le x < 1.1\\ 5.3 & \text{if } 1.1 \le x < 5.1\\ 0 & \text{if } x = 5.1 \end{cases}$$

$$(5.2)$$



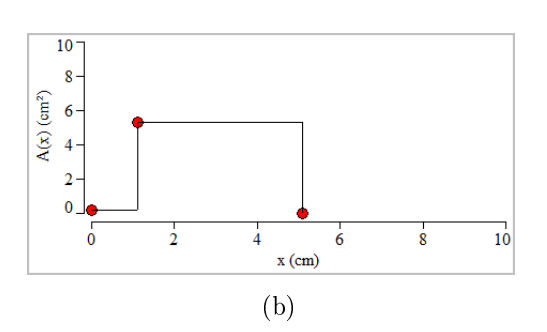


FIGURE 5.3 – (a) Design of the device used to measure the transfer function of a uniform pipe to which a resonator is connected. (b) The area function of the resonator defined by  $A_3(x)$  in equation 5.2.

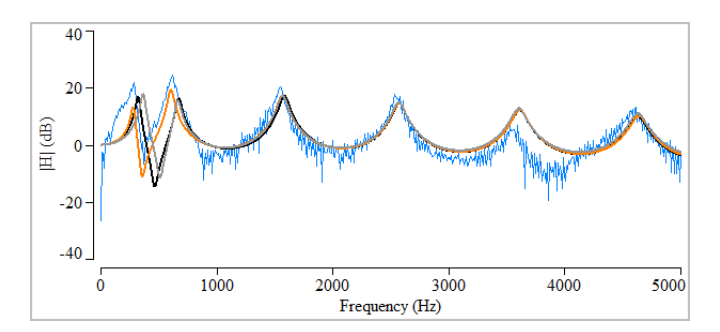
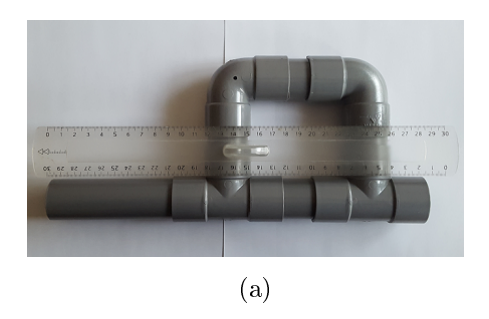


FIGURE 5.4 – Module of the transfer function  $\widetilde{H}(s)$  of a 16cm long pipe with a cross section of  $2.01cm^2$  to which is connected the resonator whose area function is plotted in (a) at x = 8.5 cm

# 5.3 Cycle zeros

Here we present an experiment in order to show that cycle zeros described in section 4.7 correspond to a physical reality. The acoustic device is an assembly of plumbing PVC pipes. A photo of the experimental device is shown in fig 5.5 (a). The acoustic graph used for modelling the experiment is shown in fig 5.5 (b).



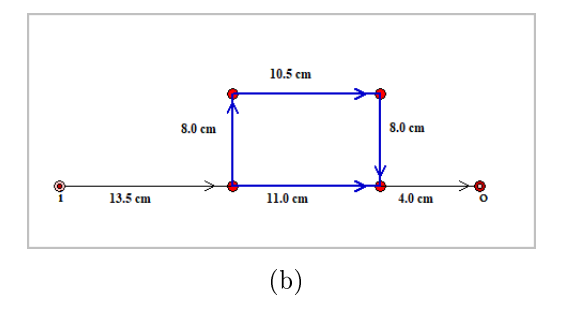


FIGURE 5.5 – (a) Experimental device made of pvc plumbing pipes. (b) The acoustic graph used to model the device. Each edge represents a pvc pipe with an area cross section of 6.16  $cm^2$  and whose length is written beside.

As in sections 5.1 and 5.2 output radiation and reacting wall parameters are adjusted by measuring the resonances of a uniform pipe. Sondhi parameters have been set to  $\omega_0 = 400 \, rad/s$ ;  $a = 400 \, rad/s$ ;  $c_1 = 10 \, rad/s$ . Output radiation parameters have been set to a = -3.3; b = 12.

We can see in fig 5.6 that we have a good matching between the computed and measured curves up to  $2700\,Hz$ .

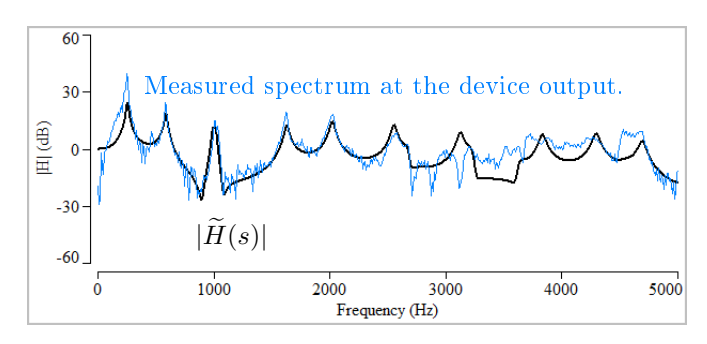


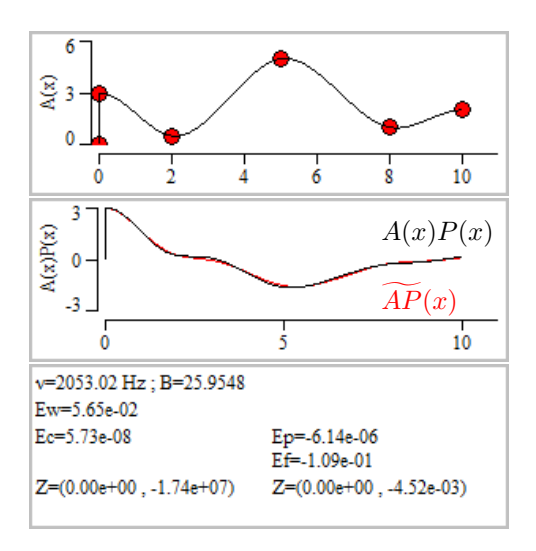
FIGURE 5.6 – Module of the transfer function  $\widetilde{H}(s)$  compared with the Fourier transform of the signal output.

# 6 Numerical schemes

We have seen at the end of sec 3.7 that the error on flow conservation on a given graph vertex remains significant once a duct connected to the vertex exhibits strong variations. Moreover, we have seen in sec 1.1 that the Webster equation holds when A(x) varies little on distances in the same order of magnitude of the pipe width. This is not the case with area functions such as defined in fig 2.1 and used in sec 3.7.

We have seen in sec 4.4 that a duct could be splitted into several parts in order to reach a good numerical precision while avoidind high degree polynomials. We also showed in sec 5.1 that, though the Webster equation does not properly describe the sound field when a duct present a sharp constriction, representing such a duct by three connected uniform pipes provide a good experimental matching.

We can see in fig 3.6 that, if we split a spline into step fuction, error terms on flow field, pressure continuity and flow conservation are reduced from several order of magnitude. Of course, this has a numerical cost: Indeed, the size of the mactrices V and W increases from 24 using the original spline area function to 124 for the modified area function where we have imposed  $0.5\,cm$  for the maximum length of individual uniform pipes.



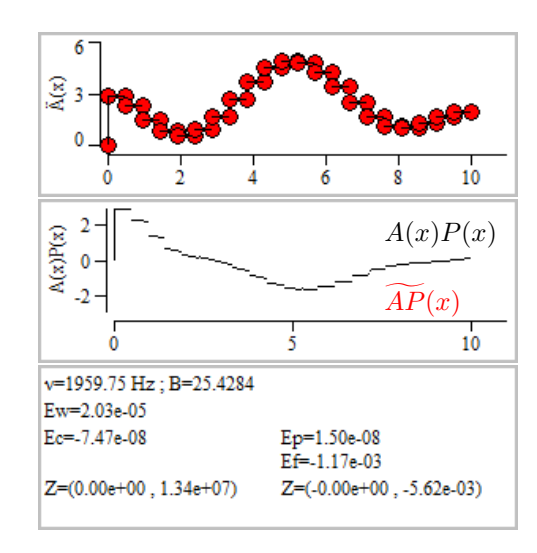


FIGURE 6.1 – Difference between computation using the original spline area function and its transformation into a concatenation of small tubes.

We can see in fig 6.2 the difference between the transfer function computed with the original or the discretized area functions.

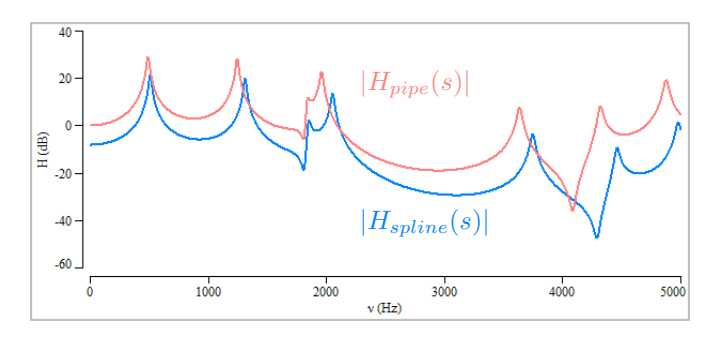


FIGURE 6.2 – Comparisond between transfer functions using left (blue) and right (red) area functions in fig 6.1

We did not realize the experiment on this geometry but, given the result obtained in sec 5.1, we think that the splitted area function should provide a better experimental matching.

# 7 Conclusions

The variational formulation of the webster equation allowed us to model the sound field in an acoustic graph composed of inteconnected acoustic ducts with variable cross section.

In section 3.3, we showed that resonance modes could obtained directly from eigenvectors of linear operators and that resonance frequencies was obtained from the corresponding eigenvalues.

In section 3.4, we showed that solutions of the Webster equation could be obtained for each value of the frequency by solving a linear system.

In section 4.5, we first identified at type of subgraphs responsible for zeros whose frequencies could also be obtained from eigen values of linear operators build with the subgraph associated area functions. In section 4.7, we showed that when cycles occur in the graph, the transfer function also contains zeros that cannot be obtained from eigen values of linear operators. Nevertheless, using the poles and zeros identified previously, we developed an algorithm for computing them at moderate numerical cost. Such zeros were observed experimentally as described in section 5.3.

In section 3.6, we showed that solutions of the Webster equation could be obtained with arbirary precision for each duct associated with graph eges but we observed in section 3.7 that errors on flow flow conservation remain significant once some of the ducts connected to a junction present strong area function variations.

Moreover, we have seen in section 5.1 that the Webster equation is not appropriated for modelling a sharp constriction, but that the variational formulation could still be used by modelling it with a concatenation of uniform pipes.

In section 6, we eventually propose a numerical scheme that allow us to model any type of acoustic graph. This sould be valid in the low frequency range where the wavelenghts are large compared to the dimension of the junction area that is not propperly modeled by our 1D formulation.

In the experimental section 5, we verified, that our calculations are in agreement with experimental results for a pipe with sharp constriction, a resonator conected to a pipe and an acoustic graph in which cycle zeros occur.

# 8 Acknowledgement

We wish to thank Geoffroy Le Grelle for manufacturing the experimental devices used in sections 5.1 and 5.2 that were also designed through his numerous advices.

# References

- [1] L Landau and E Lifchitz. *Physique théorique*, volume 6 : Mécanique des fluides. Edition MIR Moscou, second edition, 1989.
- [2] M M Sondhi. Model for wave propagation in a lossy vocal tract. J. Acoust. Soc. Amer., 55:1070–1075, 1974.
- [3] P Jospa. Des paramètres formantiques au parofil articulatoire. Actes du 12<sup>eme</sup> Congrès international des sciences phonétiques Aix-en-Provence, 2:378–381, 1991.
- [4] P Jospa, A Soquet, and M Saerens. Variational formulation of the acoustico-articulatory link and the inverse mapping by means of a neural network. *Levels in speech communication.*, pages 103–113, 1995.
- [5] R Weinstock. Calculus Of Variations. Dover, dover edition 1974 edition, 1952.
- [6] R Van Praag. Variational formulation of the sound field in branching non-uniform acoustic ducts. Application to the vocal tract. PhD thesis, Université Libre de Bruxelles ILVP, 1998.
- [7] V Smirnov. Cours de Matématiques Supérieures, volume 4. Edition MIR Moscou, 1989 2<sup>d</sup> edition, 1975.
- [8] R Van Praag and P Jospa. Variational method applied to formant computation for a pharyngo-buco-nasal tract. *Proceeding ICPhS 95 Stockholm*, 4:456–459, 1995.
- [9] P Jospa and R Van Praag. Sound field computation in a network of non-uniform ducts. application to the vocal tract. *Proceeding ICPhS 99 Stockholm*, 14:2141–2144, 1999.
- [10] J.A Bondy and U.S.R Murty. Graph Theory With Applications. North-Holland, New York Amsterdam • Oxford, 5<sup>th</sup> edition, 1982.
- [11] Alan V. Oppenheim and Ronald W. Schafer. Discrete Time Signal Processing. Prentice Hall, third (2010) edition, 1989.